RSC Advances

This is an *Accepted Manuscript*, which has been through the Royal Society of Chemistry peer review process and has been accepted for publication.

Accepted Manuscripts are published online shortly after acceptance, before technical editing, formatting and proof reading. Using this free service, authors can make their results available to the community, in citable form, before we publish the edited article. This *Accepted Manuscript* will be replaced by the edited, formatted and paginated article as soon as this is available.

You can find more information about *Accepted Manuscripts* in the Information for Authors.

Please note that technical editing may introduce minor changes to the text and/or graphics, which may alter content. The journal's standard Terms & Conditions and the Ethical guidelines still apply. In no event shall the Royal Society of Chemistry be held responsible for any errors or omissions in this *Accepted Manuscript* or any consequences arising from the use of any information it contains.

ROYAL SOCIETY OF CHEMISTRY

www.rsc.org/advances

Magnetic activated carbon prepared from rice straw-derived hydrochar for triclosan removal

Yuchen Liu[1], Xiangdong Zhu[1], Feng Qian, Shicheng Zhang*, Jianmin Chen

Shanghai Key Laboratory of Atmospheric Particle Pollution and Prevention (LAP^3), Department of Environmental Science and Engineering, Fudan University, Shanghai 200433, China

[1] These authors contributed equally to this work.

* Corresponding author.

Tel/fax: +86-21-65642297;

E-mail: zhangsc@fudan.edu.cn

RSC Advances Accepted Manuscript

Recently, considerable attention has been received in the hydrothermal liquefaction (HTL) of waste rice straw for the production of bio-oil and hydrochar. However, hydrochar material could not be directly applied in the environmental field, due to its limited porosity and surface area. In order to improve the porosity and adsorption capacity of rice straw-derived hydrochar, it was activated and magnetized to a magnetic activated carbon. The activation condition for hydrochar was firstly considered, due to the negative effect of magnetic medium. Results suggested that the as-prepared magnetic activated carbon possessed a large surface area (around 674 m^2 g^{-1}), and exhibited both high adsorption capacity and fast adsorption rate for triclosan (TCS) removal. In addition, magnetic activated carbon can be easily recovered from aqueous solutions by an external magnetic field. Overall, the waste rice straw-derived hydrochar can be transformed to a highly efficient magnetic adsorbent for TCS removal.

RSC Advances Accepted Manuscript

1. Introduction

Triclosan (TCS, 5-chloro-2-(2,4-dichlorophenoxy)-phenol), a widely used antimicrobial agent in pharmaceuticals and personal care products (PPCPs), has been received widespread public attention, due to its frequent detection in surface waters and its potential risk to human health.[1, 2] It is reported that TCS is toxic to aquatic organisms, and contributes to the generation of more toxic by-products like dioxin.[3, 4] Hence, it is of great importance to explore efficient and cost-effective treatment technologies for TCS removal from aqueous solution.

Rice straw is an abundant agriculture residue and utilized to produce bio-oil and hydrochar *via* hydrothermal liquefaction (HTL).[5-7] However, to date, more attention are focused on the production of bio-oil, with less attention paid to hydrochar.[8, 9] Rice straw-derived hydrochar is also an attractive carbon material, due to abundant oxygen-contained functional groups on its surface.[10, 11] However, the limited porosity and low surface area of hydrochar restrict the effective exploitation in environmental remediation and agricultural application.[12-14] Hence, rice straw-derived hydrochar is needed to be modified for the development of porosity.

It has been previously reported that the resultant carbons from chemical activation of hydrochar by activating agents (KOH, H_3PO_4 or $ZnCl_2$), possess large surface area and abundant pore structure.[15-17] However, little information about hydrochar activated by potassium carbonate (K_2CO_3) has been reported. K_2CO_3, a porogen with widespread application, can also activate waste carbonaceous materials to a high-porosity activated carbon, which is strongly dependent on the suitable K_2CO_3 impregnation ratio and activation temperature.[17] However, activated

RSC Advances Accepted Manuscript

carbon is difficult to be separated and recovered from aqueous solutions. Therefore, it is of great importance to employ an efficient and cost-effective technology to deal with the issue.

Generally, introducing magnetic medium to waste biomass, activated carbon or carbon nanotubes *via* hydrothermal co-precipitation reaction of ferrous and ferric ions under basic solution is a facile method to enable carbonaceous material to be efficiently separated from aqueous solutions. Nevertheless, only the magnetic carbon composite prepared from a high porosity carbonized material can retain high porosity, due to the pore-jamming effect of magnetic medium.[18-20] Then, the performance of porous structure and surface area of magnetic carbon composite is closely related to its precursor. Therefore, the optimization of activation conditions for the precursor of magnetic carbon composite should be firstly considered.

In this study, a novel magnetic activated carbon with developed porosity and high adsorption capacity has been prepared from waste rice straw-derived hydrochar via two steps. In order to enable magnetic activated carbon to possess a large surface area, the activation conditions for its precursor are firstly optimized. The main objectives of this research are to investigate the evolution of textural properties and surface chemistry between rice straw-derived hydrochar and its activated material, and to evaluate the application of the as-prepared magnetic activated carbon in TCS removal. In order to elucidate the pore-jamming effect of magnetic composition, the performances of activated carbon are also studied. It should be emphasized that few reports have been devoted to the preparation of magnetic activated carbon using this precursor.[10, 12, 13, 21]

2. Experimental

RSC Advances Accepted Manuscript

2.1 Materials

Analytical grade anhydrous potassium carbonate (K_2CO_3) and triclosan (TCS) were purchased from Sinopharm Chemical Reagent Co. Ltd. and Aladdin Reagent Corporation, respectively. Ultrapure water was generated from a Milli-Q academic water purification system (Millipore) with a resistivity of 18.2 MΩ cm^{-1}.

The rice straw-derived hydrochar material was obtained from our pilot-scale HTL unit. The HTL unit was performed using a hydrothermal reaction system (shown in Fig. S1), which consisted of a pilot-scale stainless steel autoclave, an electrically heated furnace, a magnetic stirrer, a pressure holding circuit and a controller. In a typical experimental run, 3.5 kg of rice straw and 44 L of water were placed in the autoclave and heated up to 573 K and maintained at this temperature for 30 min, followed by cooling to room temperature. The resulting solid product, denoted as hydrochar, was collected by filtration and washed with abundant ethyl acetate and distilled water, and finally dried for 4 h at 373 K.

2.2 Fabrication of magnetic activated carbon

The synthesis process of magnetic activated carbon was divided into two steps as follows: (1) fabrication of activated carbon *via* chemical activation of rice straw-derived hydrochar by K_2CO_3; (2) fabrication of magnetic activated carbon *via* the hydrothermal co-precipitation reaction. More details about the preparation process of activated carbon and magnetic activated carbon can be available in Supporting Information.

2.3 Characterization

RSC Advances Accepted Manuscript

The Brunauer-Emmett-Teller (BET) surface areas of samples were obtained from nitrogen adsorption isotherms at 77 K using a Quantasorb SI instrument (Quantachrone, USA). The X-ray diffraction (XRD) was carried out on the X'Pert PRO system equipped with a Cu Kα radiation (40 kV, 40 mA) over the 2θ range of 20-70°. The X-ray photoelectron spectroscopy analysis (XPS) were performed using a RBD upgraded PHI-5000C ESCA system (Perklin Elmer) with Mg Kα radiation ($h\nu$ = 1253.6 eV), and binding energies for the high-resolution spectra were calibrated by setting C 1s at 284.6 eV. To investigate the surface properties of as-prepared samples, the Fourier transform infrared (FT-IR) spectra were recorded in the region of 4000-400 cm^{-1} employing the KBr pellet method (Nexus 470, Nicolet). The microscopic features of samples were characterized by scanning electron microscopy (SEM, XL300, Philips) equipped with an energy-dispersive X-ray (EDX, Link 300) analyzer and transmission electron microscopy (TEM, H-600, Hitachi). The magnetic property was investigated using a vibrating sample magnetometer (VSM, Quantum).

2.4 Batch adsorption experiments

Adsorption performance of TCS on activated carbon and magnetic activated carbon were compared, in order to interpret the negative effect of magnetic composition. Batch adsorption equilibrium experiments were carried out in a set of 60 mL amber glass bottles, containing TCS solutions (20 % HPLC-grade methanol) with different initial concentrations (10 - 50 mg L^{-1}) and adsorbent (50 mg L^{-1}) on a shaker at 298 K. Adsorption kinetics of TCS onto adsorbents were performed with the initial TCS concentration of 10, 20 and 40 mg L^{-1}, respectively. After shaken

RSC Advances Accepted Manuscript

104 continuously under certain time, the solid adsorbent was separated from solutions by
105 centrifugation. Then the mixture of 1 mL obtained supernatant and 1 mL methanol was filtrated
106 by 0.45 μm polytetrafluoroethylene (PTFE) membrane filters. The amount of adsorption at
107 equilibrium (q_e, mg g^{-1}) was calculated using the following equation (equation 1):

$$q_e = \frac{(C_0 - C_e)V}{m} \quad (1)$$

108 where C_0 and C_e (mg L^{-1}) are the initial and equilibrium concentration of TCS, respectively. V (L)
109 is the volume of the solution, and m (g) is the mass of adsorbent.

110 The effect of real water was studied under initial TCS concentrations of 20 mg L^{-1} in different
111 water matrix (sea water, lake water, ground water, river water and pure water). The total organic
112 carbon (TOC) of the real water was determined with a Shimadzu TOC-L analyzer. And the effect
113 of pH on TCS adsorption was investigated in aqueous solutions over a pH range of 3-10 at initial
114 TCS concentration of 20 mg L^{-1}.

115 **2.5 HPLC analysis**

116 The TCS concentrations were determined by an Agilent 1100 HPLC with a Zorbax ODS
117 column (4.6 mm × 150 mm) at 298 K. The wavelength of ultraviolet detector was set at 280 nm,
118 and the injection volume was 50 μL. The mobile phase was a mixture of HPLC-grade methanol
119 and ultrapure water (90:10, v/v), which was delivered at 1 mL min^{-1} through the column.

120 **3. Results and discussions**

121 **3.1 Optimization of activation conditions**

122 In order to obtain a high-performance magnetic activated carbon, the optimization of

RSC Advances Accepted Manuscript

123 activation conditions for rice straw-derived hydrochar was firstly considered. Fig. S2 and S3
124 exhibit nitrogen gas (N_2) adsorption isotherms of activated carbons prepared under various
125 activation temperature and impregnation ratio (the weight ratio of K_2CO_3 to hydrochar).
126 According to the IUPAC classification, N_2 adsorption isotherms of these activated carbons
127 exhibit a combination of type I and IV, indicating the characteristics of microporous and
128 mesoporous structures.

129 As shown in Table 1, the yield of activated carbons decreased from 57.0% to 21.1% as the
130 activation temperature increased from 773 to 1073 K, due to the release of volatile products as a
131 result of intensifying dehydration and elimination reaction.[22] Accordingly, with increasing the
132 activation temperature, the BET surface area and the micropore surface area sharply increased
133 from 308 to 909 $m^2 g^{-1}$ and from 256 to 654 $m^2 g^{-1}$, respectively, due to the release of tars from
134 the cross-linked framework generated by treatment of the chemical reagents.[17] Therefore, the
135 total volume and micropore volume was obviously increased. However, the proportion of
136 micropore surface area and micropore volume gradually increased before 973 K, and then
137 decreased, partly due to the enlarging of existing micropores into mesopores.[23] Therefore, violent
138 gasification reactions occurred and decreased the microporosity at activation temperature of
139 1073 K.

140 The influence of the impregnation ratio on the characteristics of activated carbons was also
141 investigated at activation temperature of 873 K. The BET surface area, total volume and
142 micropore volume obviously increased with increasing impregnation ratio, and the proportion of

RSC Advances Accepted Manuscript

143 the micropores to the total pore volume remained steady, as indicated in Table 1.

144 **3.2 Characterization of samples**

145 In this study, the activated carbon with activation temperature 1073 K and impregnation ratio
146 2:1 was selected to prepare magnetic activated carbon, due to its high porosity. The N_2
147 adsorption isotherms and pore size distributions for hydrochar, activated carbon and magnetic
148 activated carbon are shown in Fig. S4. Obviously, hydrochar exhibited Type III isotherm,
149 suggesting that rice straw-derived hydrochar possessed less developed porous structure. After
150 activation, the isotherms for activated carbon and magnetic activated carbon presented a
151 combined feature of type I and IV curves, indicating the existence of both micropores and
152 mesopores.

153 As shown in Table 2, hydrochar presented extremely low BET surface area (6.22 $m^2 g^{-1}$) and
154 total pore volume (0.06 $cm^3 g^{-1}$). Compared with hydrochar, a remarkable increase in BET
155 surface area and pore volume (including total pore and micropore) was observable for activated
156 carbon and magnetic activated carbon, further demonstrating the importance of activation in the
157 development of pore structure. Furthermore, compared with activated carbon, the surface area of
158 magnetic activated carbon reduced from 1334 to 674 $m^2 g^{-1}$, indicating the negative effect of
159 magnetic medium. At the same time, it was found that 48.6% and 52.0% of total pore volume
160 and micropore volume, respectively, were diminished after precipitation of iron particles,
161 indicating the formation of iron particles inside the pore structure of activated carbon.[24]

162 The structure and chemical composition of the samples were determined by XRD. As seen in

RSC Advances Accepted Manuscript

Fig. 1a, the major crystalline phases for rice straw-derived hydrochar were quartz (SiO_2), weddelite ($CaC_2O_4 \cdot 2H_2O$) and whewelite ($CaC_2O_4 \cdot H_2O$). After activation, XRD peaks corresponding to different phases of calcite ($CaCO_3$) appeared in activated carbon, which can be attributed to the decomposition of weddelite and whewelite at high activating temperature. After magnetization, magnetic medium, such as goethite (peaks at 2θ = 21.2 and 35.5°), maghemite (peaks at 2θ = 35.5, 40.5, 44.6, 53.1 and 57.4°) and magnetite (peaks at 2θ = 35.5 and 61.3°), were identified as the major crystalline phase in the magnetic activated carbon.[25] To obtain further information in the surface composition for magnetic activated carbon, XPS analysis was carried out. The C 1s and O 1s spectra of magnetic activated carbon are shown in Fig. 1b and c, and the relative peak areas of C and O in different forms on the surface of magnetic activated carbon are presented in Table S1.[26, 27] It was obvious that the main functional groups containing C were C-C (284.6 eV) and O-C=O (289.0 eV). In addition, it can be deduced from the curve fitting results of O 1s spectra that, the composition ratio of magnetite (Fe_3O_4), goethite (FeO(OH)) and maghemite (γ-Fe_2O_3) was 1:2.5:1, further reflecting the presence of iron particles on the surface of carbon materials.

Fig. 1d compares the evolution of FT-IR spectra for hydrochar, activated carbon and magnetic activated carbon samples. The wide band 3400 cm^{-1}, visible for all samples, can be attributed to the -OH stretching vibrations.[21] Moreover, all samples displayed the similar adsorption band with various intensities, due to partial oxygen and carbon removal. The band at 2924/2854, 1587/1449, 1080 and 797 cm^{-1}, which were assigned to C-H stretching vibrations, skeletal C=C

RSC Advances Accepted Manuscript

vibrations, C-O bonds stretch, and out-of-plane deformation vibrations of C-H groups, respectively.[1] However, the peak at 455 cm^{-1}, assigned to the stretching vibration of Si-O-Si groups in the quartz, was only observable in hydrochar and activated carbon, but disappeared in magnetic activated carbon, which was in good agreement with the results of XRD analysis. Accordingly, magnetic activated carbon exhibited an additional band at 583 cm^{-1}, compatible with the presence of iron oxide in the sample.[19]

Details about the structure and morphology of the obtained samples were examined in the SEM and TEM observations (shown in Fig. 2). The surface of hydrochar appeared rough, with rarely rudimentary pores due to the preliminary constitute decomposition (Fig. 2a).[18] After activation, numerous surface pores were produced, contributing to the increase of the surface area (Fig. 2b).[4] Further magnetization, the iron oxide or hydroxide particles covered the surface of activated carbon, blocking the pores (Fig. 2c).[28] These results well agree with the data of surface areas from Table 2. And the TEM images confirmed that developed porosity was formed in activated carbon, compared with hydrochar (Fig. 2d, e).

To evaluate the magnetic behavior of magnetic activated carbon, the magnetic measurements were carried out at 300 K. According to hysteresis loop (Fig. S5), the saturation magnetization of magnetic activated carbon was measured to be 12.4 emu g^{-1}, indicating a superparamagnetic behavior. This implied that magnetic activated carbon can be easily recovered by an external magnetic field (Fig. S5, inset), thus providing a potential advantage for the separation of adsorbents.[24]

RSC Advances Accepted Manuscript

3.3 Adsorption studies

3.3.1 Adsorption isotherms

Adsorption isotherm is basically important to describe how adsorbates interact with adsorbents, and is critical in optimizing the use of adsorbents. In this study, two widely used isotherm models (the Langmuir model and Freundlich model) were employed to describe the adsorption process. The Langmuir model (Eq. (2)) and Freundlich model (Eq. (3)) can be represented as follows:

$$C_e/q_e = 1/q_m K_L + C_e/q_m \quad (2)$$

$$\ln q_e = \ln K_F + (1/n) \ln C_e \quad (3)$$

where q_m is the maximum adsorption capacity (mg g^{-1}), K_L is a constant related to free energy or adsorption enthalpy (L mg^{-1}), K_F is related to the adsorption capacity of the adsorbent ($mg^{(1-1/n)}$ g^{-1} $L^{1/n}$), and 1/n is another constant related to the surface heterogeneity.

The Langmuir and Freundlich parameters, together with regression coefficients, in adsorption of TCS onto activated carbon and magnetic activated carbon are listed in Table 3. As indicated in Fig. S6, the adsorption of TCS onto activated carbon and magnetic activated carbon was well fitted with Langmuir model, in accordance with the correlation coefficient (R^2) values obtained from Table 3. It was evident that the adsorption capacity of TCS on activated carbon, was significantly greater than that on magnetic activated carbon, indicating that the adsorption process was mainly dependent upon surface area and porosity of adsorbents and further demonstrating the negative effect of magnetic medium.[29] Compared with the TCS adsorption capacities of various previously known adsorbents (Table S2), magnetic activated carbon

RSC Advances Accepted Manuscript

exhibited an excellent adsorption performance.[1, 3, 30, 31]

For the Langmuir model, to determine whether the adsorption system is favorable or not, the isotherm can be classified by the separation factor (R_L), which is represented by the following equation:

$$R_L = \frac{1}{1+K_L C_0} \quad (4)$$

The value of K_L is listed in Table 3. The R_L parameter gives important signs on the possibility of the adsorption process that might be irreversible (R_L=0), favorable (0 < R_L < 1), linearity of adsorption (R_L=1) or unfavorable (R_L >1). In the present work, the R_L values were found within the range of 0.02-0.04, demonstrating that TCS adsorption onto activated carbon and magnetic activated carbon was favorable.

3.3.2 Adsorption kinetics

In order to investigate the rate of TCS adsorption, three different kinetic models, i.e. the pseudo first-order model (Eq. (5)), pseudo second-order model (Eq. (6)) and Elvoich equation (Eq. (7)),[32] were applied to simulate the kinetics of TCS adsorption onto activated carbon and magnetic activated carbon.

$$q_t = q_e\left(1-e^{-k_1 t}\right) \quad (5)$$

$$\frac{t}{q_t} = \frac{1}{k_2 q_e^2} + \frac{t}{q_e} \quad (6)$$

$$q_t = \left(\frac{1}{b}\right)\ln(ab) + \left(\frac{1}{b}\right)\ln t \quad (7)$$

where q_t is the amount of TCS adsorbed at time t (mg g^{-1}); k_1 (min^{-1}) and k_2 (g mg^{-1} min^{-1}) are the pseudo first-order and pseudo second-order rate constant, respectively; a is the initial adsorption

RSC Advances Accepted Manuscript

237 rate constant (mg g^{-1} min^{-1}) and b is related to the extent of surface coverage and activation
238 energy for chemisorption (g mg^{-1}).

239 The adsorption kinetics parameters are listed in Table 4. Obviously, the pseudo second-order
240 equation agreed well with the data for $R^2 \geqslant 0.99$. Additionally, the $q_{e,cal}$ from pseudo
241 second-order model were close to the experimental values $q_{e,exp}$. Therefore, the pseudo
242 second-order model was the best for predicting the adsorption kinetics of TCS onto activated
243 carbon and magnetic activated carbon.

244 As shown in Fig. S7, it is apparent that it took much more time to achieve the adsorption
245 equilibrium with higher initial concentration, implying that the adsorption occurred at first on the
246 exterior surface of adsorbents, followed by the interior surface. It should be noted that magnetic
247 activated carbon showed very fast adsorption rate, which can be described by the
248 pseudo-second-order kinetic model with its kinetic rate (around 5×10^{-4} g mg^{-1} min^{-1}).

249 Besides, to investigate the diffusion mechanism and elucidate rate-determining steps towards
250 simulated adsorption, the intraparticle diffusion model was applied to obtain insight into the
251 adsorption process and the equation was described as follows:

$$q_t = k_{id} t^{1/2} + c \qquad (9)$$

252 where k_{id} (mg g^{-1} $min^{-0.5}$) is the intra-particle diffusion rate constant, and c (mg g^{-1}) is a constant
253 related to boundary layer thickness.

254 If the intraparticle diffusion curve passes through the origin, then the intraparticle diffusion is
255 the sole rate-limiting step. Or else, the adsorption process is controlled by some degree of

RSC Advances Accepted Manuscript

boundary layer.[33] As seen from Fig. 3 and Table S3, the curve was multi-linear and did not pass through the origin, implying that a rapid diffusion took place on the external surface of the adsorbent at first, followed by intraparticle diffusion of TCS, through which TCS molecules were migrated toward the sites where actual adsorption took place.[34]

3.3.3 Effect of water matrix

The effect of solution pH on the TCS adsorption by activated carbon and magnetic activated carbon were carefully investigated in the pH value of 3-10. As shown in Fig. 4a, the adsorption capacity of TCS gradually decreased with an increase in pH at initial TCS concentration of 20 mg L^{-1}. It is partly attributed to electrostatic repulsion between deprotonated TCS and the negatively charged adsorbent surface.[3] Moreover, the adsorption capacity of magnetic activated carbon was more sensitive to solution pH than that of activated carbon.

Real waters spiked with the initial TCS concentration of 20 mg L^{-1} were used to further evaluate the effect of different matrix on the TCS adsorption. Clearly, the amounts of TCS adsorbed on activated carbon and magnetic activated carbon in pure water are relatively larger than that obtained in other water matrix (Fig. 4b). Generally, high pH and concentration of humic acid (HA) could inhibit the adsorption of TCS, as confirmed by Fig. 4a and Fig. S8.[35] Hence, it could be deduced that lower concentration of TOC as well as the lower solution pH of pure water would result in its higher adsorption capacity for TCS removal from aqueous solution (Table S4). Overall, magnetic activated carbon can act as an excellent adsorbent for TCS in real water matrix.

RSC Advances Accepted Manuscript

4. Conclusions

A novel magnetic activated carbon with developed porosity and excellent triclosan adsorption performance was synthesized from waste rice straw-derived hydrochar *via* activation and subsequent magnetization method. The increase in the activation temperature and the impregnation ratio promoted the development of porosity of activated carbon, which was closely associated to that of magnetic activated carbon. The spent magnetic activated carbon can be easily recovered by an external magnetic field. Compared to other known adsorbents, the as-prepared magnetic activated carbon possessed superior TCS adsorption capacity and fast adsorption rate. The present study indicated that the waste rice straw-derived hydrochar was a promising precursor for the synthesis of high-performance magnetic activated carbon in the removal of contaminants from real water matrix.

Acknowledgements

This research was supported by the National Natural Science Foundation of China (No. 21407027). The authors also thank the anonymous reviewers for fruitful suggestions.

Appendix A. Supplementary data

Supplementary data associated with this article can be found on the online version.

RSC Advances Accepted Manuscript

References

1 C. Lei, Y.-Y. Hu and M.-Z. He, *Chem. Eng. J.*, 2013, **219**, 361-370.

2 K. Murugesan, V. Bokare, J. R. Jeon, E. J. Kim, J. H. Kim and Y. S. Chang, *Bioresour. Technol.*, 2011, **102**, 6019-6025.

3 S. K. Behera, S. Y. Oh and H. S. Park, *J. Hazard. Mater.*, 2010, **179**, 684-691.

4 X. Zhu, Y. Liu, G. Luo, F. Qian, S. Zhang and J. Chen, *Environ. Sci. Technol.*, 2014, **48**, 5840-5848.

5 A. Rodríguez, A. Moral, R. Sánchez, A. Requejo and L. Jiménez, *Bioresour. Technol.*, 2009, **100**, 4863-4866.

6 X. Z. Yuan, H. Li, G. M. Zeng, J. Y. Tong and W. Xie, *Energy*, 2007, **32**, 2081-2088.

7 K. Murakami, K. Kasai, T. Kato and K. Sugawara, *Fuel*, 2012, **93**, 37-43.

8 D. Zhou, L. Zhang, S. Zhang, H. Fu and J. Chen, *Energ. Fuel.*, 2010, **24**, 4054-4061.

9 C. J. Li, X. Yang, Z. Zhang, D. Zhou, L. Zhang, S. C. Zhang and J. M. Chen, *Bioresources*, 2013, **8**, 2981-2997.

10 E. Unur, *Micropor. Mesopor. Mater.*, 2013, **168**, 92-101.

11 W. J. Liu, F. X. Zeng, H. Jiang and X. S. Zhang, *Bioresour. Technol.*, 2011, **102**, 8247-8252.

12 C. Falco, J. P. Marco-Lozar, D. Salinas-Torres, E. Morallón, D. Cazorla-Amorós, M. M. Titirici and D. Lozano-Castelló, *Carbon*, 2013, **62**, 346-355.

13 M. Sevilla, A. B. Fuertes and R. Mokaya, *Energ. Environ. Sci.*, 2011, **4**, 1400-1410.

14 X. Zhu, Y. Liu, C. Zhou, G. Luo, S. Zhang and J. Chen, *Carbon*, 2014, **77**, 627-636.

15 M. Sevilla and A. B. Fuertes, *Energ. Environ. Sci.*, 2011, **4**, 1765-1771.

16 L. Wang, Y. Guo, B. Zou, C. Rong, X. Ma, Y. Qu, Y. Li and Z. Wang, *Bioresour. Technol.*, 2011, **102**, 1947-1950.

17 D. Angin, E. Altintig and T. E. Kose, *Bioresour. Technol.*, 2013, **148**, 542-549.

18 X. Zhu, Y. Liu, F. Qian, C. Zhou, S. Zhang and J. Chen, *Bioresour. Technol.*, 2014, **154**, 209-214.

19 D. Mohan, A. Sarswat, V. K. Singh, M. Alexandre-Franco and C. U. Pittman, *Chem. Eng. J.*, 2011, **172**, 1111-1125.

20 M. Zhang, B. Gao, S. Varnoosfaderani, A. Hebard, Y. Yao and M. Inyang, *Bioresour. Technol.*, 2013, **130**, 457-462.

21 S. Román, J. M. Valente Nabais, B. Ledesma, J. F. González, C. Laginhas and M. M. Titirici, *Micropor. Mesopor. Mater.*, 2013, **165**, 127-133.

22 D. Adinata, W. M. Wan Daud and M. K. Aroua, *Bioresour. Technol.*, 2007, **98**, 145-149.

23 I. I. Gurten, M. Ozmak, E. Yagmur and Z. Aktas, *Biomass Bioenerg.*, 2012, **37**, 73-81.

RSC Advances Accepted Manuscript

24 M. H. Do, N. H. Phan, T. D. Nguyen, T. T. Pham, V. K. Nguyen, T. T. Vu and T. K. Nguyen, *Chemosphere*, 2011, **85**, 1269-1276.

25 L. C. Oliveira, R. V. Rios, J. D. Fabris, V. Garg, K. Sapag and R. M. Lago, *Carbon*, 2002, **40**, 2177-2183.

26 Y. Gao, X. Wang, J. Wang, X. Li, J. Cheng, H. Yang and H. Chen, *Energy*, 2013, **58**, 376-383.

27 J. Guo, R. Wang, W. W. Tjiu, J. Pan and T. Liu, *J. Hazard. Mater.*, 2012, **225-226**, 63-73.

28 T. Depci, *Chem. Eng. J.*, 2012, **181–182**, 467-478.

29 T. R. Bastami and M. H. Entezari, *Chem. Eng. J.*, 2012, **210**, 510-519.

30 S. Zhou, Y. Shao, N. Gao, J. Deng and C. Tan, *Clean - Soil, Air, Water*, 2013, **41**, 539-547.

31 J. López-Morales, O. Perales-Pérez and F. Román-Velázquez, *Adsorpt. Sci. Technol.*, 2012, **30**, 831-846.

32 H. Y. Zhu, Y. Q. Fu, R. Jiang, J. H. Jiang, L. Xiao, G. M. Zeng, S. L. Zhao and Y. Wang, *Chem. Eng. J.*, 2011, **173**, 494-502.

33 T.-T. Li, Y.-G. Liu, Q.-Q. Peng, X.-J. Hu, T. Liao, H. Wang and M. Lu, *Chem. Eng. J.*, 2013, **214**, 189-197.

34 B. H. Hameed and A. A. Rahman, *J. Hazard. Mater.*, 2008, **160**, 576-581.

35 J.-F. Liu, Z.-S. Zhao and G.-B. Jiang, *Environ. Sci. Technol.*, 2008, **42**, 6949-6954.

RSC Advances Accepted Manuscript

Figure captions:

Fig. 1 (a) X-ray powder diffraction (XRD) patterns of hydrochar (HC), activated carbon (AC) and magnetic activated carbon (MAC). X-ray photoelectron spectroscopy (XPS) spectra of magnetic activated carbon: (b) C1s high-resolution spectra, (c) O1s high-resolution spectra. (d) FT-IR spectra of hydrochar (HC), activated carbon (AC) and magnetic activated carbon (MAC).

Fig. 2 SEM images of (a) hydrochar (HC), (b) activated carbon (AC), (c) magnetic activated carbon (MAC), and TEM images of (d) hydrochar (HC) and (e) activated carbon (AC).

Fig. 3 Intraparticle diffusion kinetics for adsorption of TCS onto (a) activated carbon and (b) magnetic activated carbon at 298 K under different initial concentrations.

Fig. 4 (a) Effect of real water matrix on TCS adsorption onto activated carbon (AC) and magnetic activated carbon (MAC) at initial TCS concentration of 20 mg L^{-1}. (b) Effect of solution pH on TCS adsorption onto activated carbon (AC) and magnetic activated carbon (MAC) at initial TCS concentration of 20 mg L^{-1}.

RSC Advances Accepted Manuscript

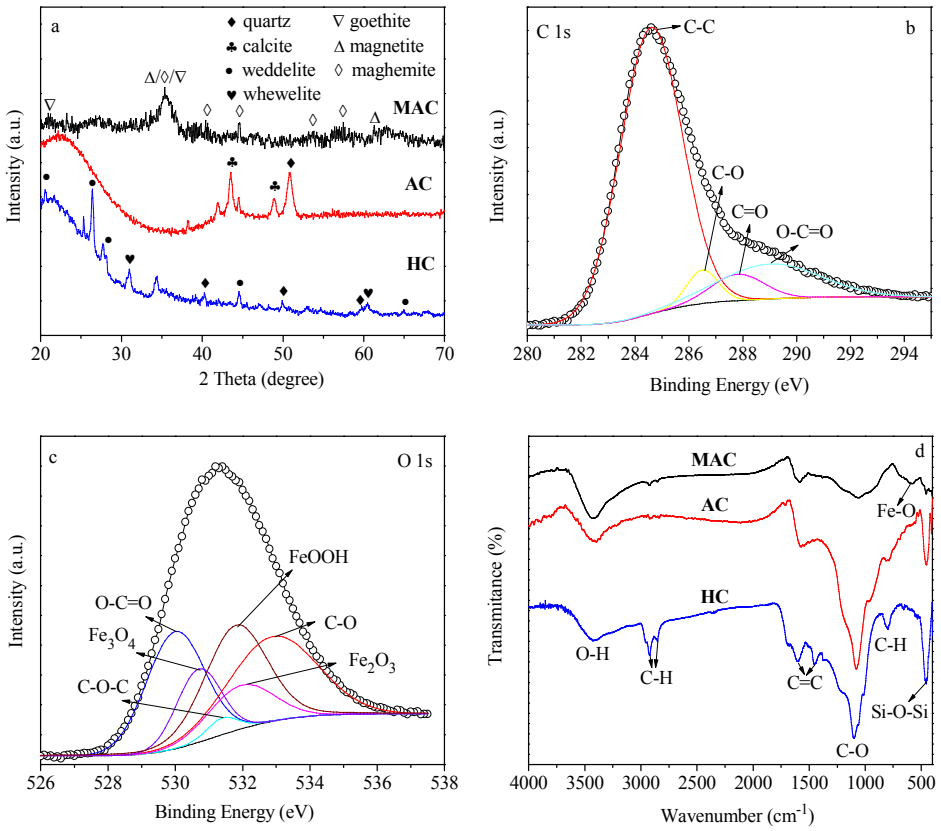

Fig. 1

RSC Advances Accepted Manuscript

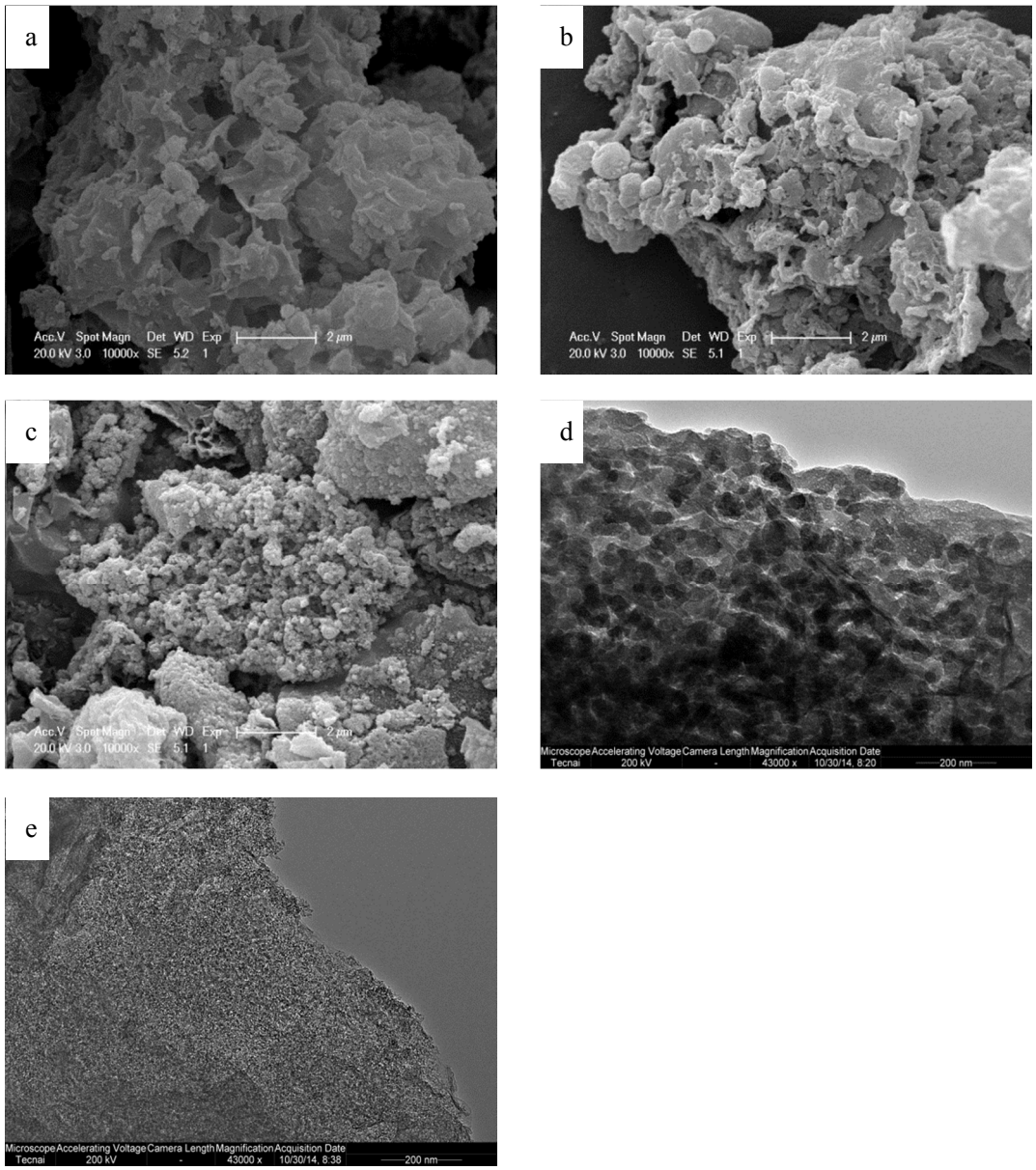

Fig. 2

RSC Advances Accepted Manuscript

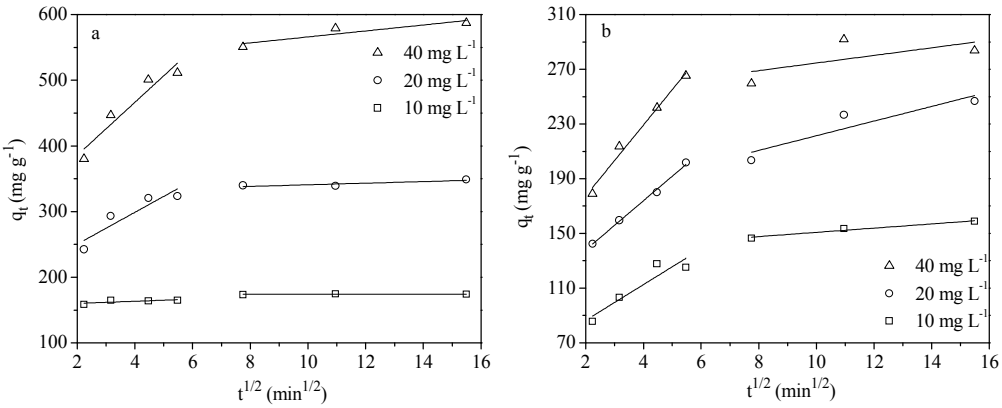

Fig. 3

RSC Advances Accepted Manuscript

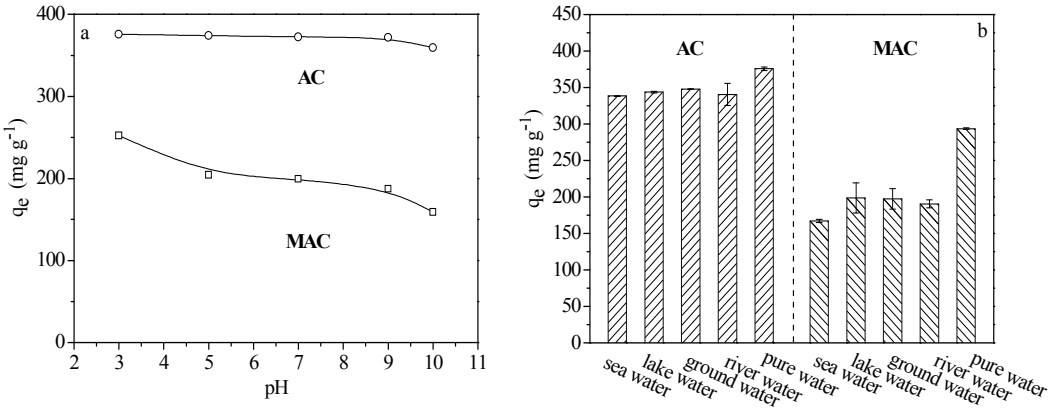

Fig. 4

RSC Advances Accepted Manuscript

Table 1 Textural properties of activated carbons prepared under different temperatures and impregnation ratios

Temperature (K)	Impregnation ratio [a]	Yield [b] (%)	S_{BET} [c] ($m^2 g^{-1}$)	S_{mic} [d] ($m^2 g^{-1}$)	S_{mic}/S_{BET}	V_T [e] ($cm^3 g^{-1}$)	V_{mic} [f] ($cm^3 g^{-1}$)	V_{mic}/V_T
773	2	57.0	308	256	0.83	0.26	0.13	0.50
873	2	49.9	506	437	0.86	0.41	0.22	0.54
973	2	30.8	697	595	0.85	0.49	0.29	0.59
1073	2	21.1	909	654	0.72	0.72	0.32	0.44
873	0.5	50.7	404	351	0.87	0.32	0.18	0.56
873	1	51.0	489	430	0.88	0.38	0.22	0.58
873	4	45.3	549	474	0.86	0.42	0.24	0.57

[a] The weight ratio of K_2CO_3 to hydrochar. [b] The weight ratio of activated carbon to hydrochar. [c] Measured using N_2 adsorption with the Brunauer-Emmett-Teller (BET) method. [d] Micropore surface area calculated using the *t*-plot method. [e] Total pore volume determined at P/P_0=0.99. [f] Micropore volume calculated using the *t*-plot method.

RSC Advances Accepted Manuscript

Table 2 Textural properties for hydrochar (HC), activated carbon (AC) and magnetic activated carbon (MAC) samples

Sample	S_{BET} [a] ($m^2 g^{-1}$)	S_{mic} [b] ($m^2 g^{-1}$)	S_{mic}/S_{BET}	V_T [c] ($cm^3 g^{-1}$)	V_{mic} [d] ($cm^3 g^{-1}$)	V_{mic}/V_T
HC	6.22	-	0	0.06	-	0
AC	1334	1010	0.76	1.07	0.50	0.47
MAC	674	484	0.72	0.72	0.24	0.33

[a] Measured using N_2 adsorption with the Brunauer-Emmett-Teller (BET) method. [b] Micropore surface area calculated using the *t*-plot method.[c] Total pore volume determined at P/P_0=0.99.[d] Micropore volume calculated using the *t*-plot method.

RSC Advances Accepted Manuscript

Table 3 Adsorption equilibrium constants obtained from Langmuir and Freundlich isotherms in the adsorption of TCS onto activated carbon (AC) and magnetic activated carbon (MAC) at 298K (q_m: mg g^{-1}, K_L: L mg^{-1}, K_F: $mg^{(1-1/n)}$ g^{-1} $L^{1/n}$)

	Langmuir				Freundlich		
Sample	q_m	K_L	R_L	R^2	K_F	n	R^2
AC	714	0.52	0.04	0.97	232	2.25	0.64
MAC	303	0.89	0.02	0.99	150	4.68	0.91

RSC Advances Accepted Manuscript

Table 4 Kinetic parameters obtained from kinetic models for the adsorption of TCS onto activated carbon (AC) and magnetic activated carbon (MAC) at 298 K (C_0: mg L^{-1}, $q_{e,exp}$: mg g^{-1}, $q_{e,cal}$: mg g^{-1}, k_1:min^{-1}, k_2: g mg^{-1} min^{-1}, a: mg g^{-1} min^{-1}, b: g mg^{-1})

			Pseudo-first-order			Pseudo-second-order			Elovich		
Sample	C_0	$q_{e,exp}$	$q_{e,cal}$	k_1	R^2	$q_{e,cal}$	k_2	R^2	a	b	R^2
AC	10	174	8.94	0.014	0.52	175	0.0066	0.99	1.8×10^{16}	0.24	0.87
	20	349	67.7	0.023	0.93	357	0.0012	0.99	3.1×10^{5}	0.04	0.81
	40	587	167	0.023	0.99	588	0.0004	0.99	2.3×10^{4}	0.02	0.94
MAC	10	159	63.8	0.022	0.99	161	0.0010	0.99	4.6×10^{2}	0.05	0.95
	20	247	120	0.023	0.98	250	0.0005	0.99	9.7×10^{2}	0.04	0.98
	40	292	44.9	0.017	0.26	286	0.0010	0.99	6.8×10^{3}	0.04	0.88

RSC Advances Accepted Manuscript